Simulation of natural convection effects on succinonitrile crystals

Robert Tönhardt and Gustav Amberg
Department of Mechanics, Royal Institute of Technology (KTH), S-100 44 Stockholm, Sweden
(Received 3 June 1999)

A numerical study of the effect of natural convection on the growth of succinonitrile crystals has been performed. All simulations are two-dimensional phase-field computations using an adaptive finite element method. The undercooling has been varied between 1.92 to 0.12 K, which is within the range used in experiments. The thermal natural convection has minor effects at 1.92 K, but the influence increases with decreasing undercooling, due to the fact that the size of the crystal increases. The simulation results show a decrease of the growth Peclet number with decreasing undercooling that is very similar to that observed in terrestrial experiments. Also, the simulation results for the orientation effect of the gravity vector agree qualitatively with experiments.

PACS number(s): 44.25.+f, 02.60.Cb, 02.70.Dh, 47.15.Cb

I. INTRODUCTION

When a nucleus solidifies in an undercooled melt, the size, morphology, growth rate, etc. may be strongly affected by any motion in the melt. This motion will thus be important for the properties of the finished material. Such melt flows may be due, for instance, to imposed external stirring, flow induced by solidification shrinkage, or a large scale convection in the bulk melt due to imposed temperature gradients. Another cause, that will be investigated here, is the natural convection that may result from the release of latent heat from the growing crystal. Considering an undercooled melt with dendritic solidification from an isolated nucleus, the adjacent melt is heated by the released latent heat, and the corresponding change in density may cause gravitational convection. The ensuing melt flow may alter the local heat transfer around the tip, and this may have large effects on the growth of the dendrite.

In the last decades there has been some interest in natural convection effects on the morphology and growth of individual dendrites. A recent review is available in Ref. [1]. One reason for this interest is that natural convection is frequently suspected to influence experimental results [2–6]. For pure succinonitrile (SCN) there are quantitative measurements [2–4,7,8] of the velocities and radii of the tips of the main stems. Experimental and theoretical work has shown that the effects of natural convection increase at low undercooling, due to the increasing size of the dendrites [9]. One indication of this is that when terrestrial measurements are compared to theories that disregard convection, such as the classical Ivantsov theory [10], the agreement is good only for a small interval of undercooling. For undercooling above 4–5 K, there seems to be interface kinetic effects. For growth below this undercooling, but above 2 K, the Ivantsov solution agrees well with experiments. Moreover, the Ivantsov solution, in combination with a constant value of the stability parameter, gives a theoretical tip velocity and tip radius that are almost the same as those measured in terrestrial experiments. Below 2 K the terrestrial growth again deviates from this theoretical operation point of the tip. Under terrestrial conditions it has also been observed that the dendritic growth depends on the direction of the gravitational field. The side branches close to the tip of the dendrite and the operation point of the tip change depending on the growth direction relative to gravity. Also, it has been found that the operating point of the tip of a dendrite is different in terrestrial and microgravity experiments. It has also been shown that the volume-change at the solid-liquid interface which results in a Stefan wind has only a minor effect on the operating point of the tip [11,12].

In a microgravity environment it was observed [3,8] that some nondiffusive phenomena may affect the growth at high undercooling, which is probably a result of the kinetic effects at the phase-interface. Ananth and Gill [13] suggested that the reason for the overprediction of the growth velocity of the isothermal dendrite theory, for undercooling above 0.23 K, is due to a Stefan wind and the Gibbs-Thompson effect. Also, at lower undercooling, the experimental results deviate from Ivantsov's transport theory [10].

A modification by Pines *et al.* [11] is attributed to the finite size of the experimental chamber. The proximity of the walls is included by looking at the distance between the tip and the closest chamber wall. It was concluded [11,14] that the finite size of the container may be of importance in micro-gravity. Both of these new theories agree with Glicksman's isothermal dendritic growth experiments (IDGE). Tennenhouse *et al.* [15] also compared the new theories with the IDGE experimental results, and it seems that the wall proximity effect is the main reason for the discrepancy between the theory and the microgravity experiments at low undercooling. It should be noted that the use of Ivantsov's transport solution is a weakness, and partly responsible for differences between theory and experiments.

The case of immediate interest in this paper, natural convection, was studied theoretically primarily by asymptotic methods. Gill and co-workers investigated the effects of forced and natural convection on dendrite growth in a series of papers [7,9,13,16,17], using an approximation that is valid close to the dendrite tip. Ananth and Gill [9] used this to solve the Navier-Stokes equations with thermal buoyancy for a shape preserving paraboloidal dendrite tip, and computed, for instance, the growth Peclet number as a function of undercooling. They showed, somewhat unexpectedly, that natural convection becomes important for sufficiently small undercooling, and that the tip radius of the dendrite is the

characteristic length scale for the thermal convection. Canright and Davis [18] used a different approximation, which assumes, a small buoyancy, but is valid in a larger region around the tip. They studied, among other things, the influence of the Prandtl number. Sekerka *et al.* [19] introduced the natural convection fluid flow by replacing the dendrite array by an isothermal sphere that encloses the dendrites, and then treating the case of the sphere surrounded by cold melt. The stagnant thermal boundary layer around the sphere is then used to modify the Nusselt number for the tip of a dendrite.

In this paper the phase-field method proposed by Karma and Rappel [20,21] is used to track the solid-liquid interface. In this method the parameters can be adjusted to give arbitrary interface kinetics. Moreover, the interface can be rather wide, and the method still gives accurate results. This method was used by many researchers [22–24]. Provatas *et al.* [23], and Braun and Murray [25], used the finite element method (FEM) with adaptivity. Provatas *et al.* [23] have performed, among other things, a long time computation of thermal growth of a free two-dimensional (2D) dendrite for the dimensionless undercooling of 0.1. Provotas *et al.* [26] computed 2D dendrites down to an undercooling of 0.05, and investigated time dependent growth at low undercooling.

Phase-field simulations with convection were performed only very recently. Tong *et al.* [22] made computations with forced fluid flow toward a free thermal dendrite. Convection effects on a dendrite growing into a shear flow were studied by the authors [27,28]. However, to our knowledge there are no published phase-field simulations of natural convection effects on dendritic growth.

The purpose of the present paper is to study how natural convection affects the evolution of a crystal. We have simulated growth of a thermal dendrite of pure SCN in two dimensions. In the following, the mathematical problem is formulated in Sec. II, the numerical aspects are discussed in Sec. III, and the results are presented in Sec. IV.

II. MATHEMATICAL FORMULATION

A rectangular chamber filled with a pure single-component melt is considered. The melting temperature of the material is T_m, and it is initially at a uniform temperature T_∞. The melt is undercooled, i.e., $T_m > T_\infty$. The walls of the chamber are maintained at a constant temperature T_∞. In the center of the chamber a nucleus is placed, and it is assumed to be held fixed during the subsequent growth. Initially the nucleus is assumed to be circular with a nondimensional radius of 5, and to be at the melting temperature T_m.

A sketch of the computational domain is shown in Fig. 1. It represents the right half of the chamber. On the left boundary of the domain, where the nucleus is positioned, symmetry boundary conditions are applied, as indicated in the figure. It is thus assumed in the simulations that the nucleus grows symmetrically with respect to the vertical centerline. On the right, top, and bottom boundaries, solid isothermal walls are assumed, as indicated.

The dimensionless time, spatial coordinates, temperature, flow velocity, and pressure are denoted by t, (x,y), θ, $\bar{u}$, and p, respectively. The length and time have been scaled with a

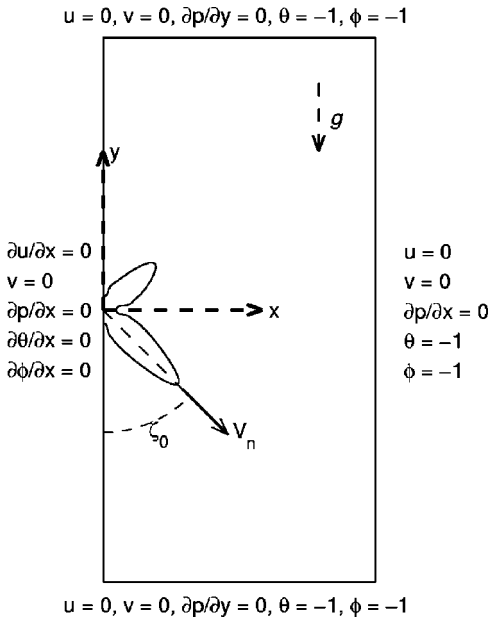

FIG. 1. A sketch of the domain of computation with boundary conditions. The contour represents the solid-liquid interface of the crystal. The angle ζ_0 denotes the angle between the direction of gravity and the preferred growth direction. u and v are the velocity components in the x and y directions respectively, and V_n is the tip speed.

reference length W, and the thermal diffusion time W^2/α, respectively, where α is the thermal diffusivity. Velocities have been scaled with the diffusion velocity α/W. The pressure has been scaled with $\rho_0 \alpha \nu_0 / W^2$, where ρ_0 and ν_0 are the reference density and viscosity at $T = T_m$, respectively. The nondimensional temperature has been introduced as $\theta = (T - T_m)/(T_m - T_\infty)$, where T is the dimensional temperature.

All the material properties are assumed to be the same in both the liquid and solid phases, except for the density. The solid phase has a constant density ρ_0, while the density of the fluid, ρ, varies with temperature as

$$\rho = \rho_0[1 - \beta(T - T_\infty)]. \tag{1}$$

Here β is the thermal expansion coefficient. The relevant material parameters that were used ib this study are listed in Table I.

In both the solid and liquid phases the energy equation is written as

$$\frac{\partial \theta}{\partial t} + \bar{u} \cdot \nabla \theta = \frac{1}{2\Delta} \frac{\partial \phi}{\partial t} + \nabla^2 \theta. \tag{2}$$

Here $\Delta = (T_m - T_\infty)/(L/c_p)$ is the dimensionless undercooling. L is the latent heat, and c_p is the specific heat of the material. Hence Eq. (2) models the heat equation in the solid ($\bar{u} = 0$) and liquid phases. It also models the release of latent heat at the solid-liquid interface. This equation was derived phenomenologically in Refs. [22,27].

In formulating the equations for the melt flow, the Boussinesq approximation has been used, as is often done in heat transfer research. This amounts to neglecting the density variations with temperature everywhere except in the gravity

TABLE I. The material properties of SCN.

Symbols	Meaning	Value
T_m	Melting temperature	331.23 K
c_p	Specific heat	1.99 J/(cm^3 K)
L	Latent heat of fusion	47.8 J/cm^3
α	Diffusivity	1.12×10^{-3} cm^2/s
k	Conductivity	2.23×10^{-3} J/(cm s K)
ρ_0	Density	1.0 g/cm^3
β	Thermal expansion coefficient	8.1×10^{-4} K^{-1}
σ_0	Surface energy	8.9×10^{-7} J/cm^2
ν_0	Kinematic viscosity	0.026 cm^2/s
ϵ	Degree of anisotropy	0.015

force term in the momentum balance, and also neglecting the temperature variations of other material properties. It can easily be shown that this is a consistent approximation that is valid for small relative density differences, which, using Eq. (1), can be estimated here to be $\beta(T_m-T_\infty)$. With representative numbers ($T_m-T_\infty<2$ K), this is always less than 1.6×10^{-3}

Due to the Boussinesq approximation, and the assumption of equal densities of melt and solid, the continuity equation can be written as

$$\nabla\cdot\overline{u}=0. \tag{3}$$

The fluid flow is governed by the Navier-Stokes equations, in the following form, where the Boussinesq approximation has been used:

$$\frac{1}{\mathrm{Pr}}\left(\frac{\partial\overline{u}}{\partial t}+\overline{u}\cdot\nabla\overline{u}\right)=\nabla p+\nabla\cdot(f_\nu[\nabla\overline{u}+(\nabla\overline{u})^*])+\mathrm{Ra}\,\theta\hat{y}. \tag{4}$$

Here $\mathrm{Pr}=\nu_0/\alpha$ is the Prandtl number, the asterisk denotes the transpose operator, and $\mathrm{Ra}=g\beta W^3(T_m-T_\infty)/(\alpha\nu_0)$ is the Rayleigh number.

With the assumption that the melt and solid have the same density, the atoms are at rest in the solid, and there is no volume flow at the interface. Therefore, the fluid velocity must become zero when approaching the solid-liquid interface, as with the no slip condition usually applied at a solid surface. This boundary condition can not be applied directly, since the solid-liquid interface is tracked implicitly through the phase-field variable. Instead the no slip condition is implemented by explicitly setting the velocity to zero in the nodes of the computational mesh, with a value $\phi\geqslant0.5$, and by making the viscosity a rapidly increasing function of the phase field ϕ.

This viscosity increase is introduced via the function f_ν of the phase-field variable ϕ that appears in Eq. (4). We have used the following definition of f_ν:

$$f_\nu=\begin{cases}1 & \phi<-0.6\\ 1+10\,(\phi+0.6)^2 & \text{otherwise.}\end{cases} \tag{5}$$

The simulation result is rather insensitive to variation of f_ν and $f_\nu\equiv1$ gives only a small decrease in accuracy.

Diepers *et al.* [29], and Tong *et al.* [22] suggested another way to implement the no slip condition on the solidification interface. They modified the Navier-Stokes equation by adding a volumetric shear dissipation term, which is switched on in the solid region. They also made this more accurate than the method used here. However, since the mesh is extremely fine close to the interface, we have been satisfied with the above.

The solid-liquid interface is tracked by the phase-field equation

$$\tau w^2\frac{\partial\phi}{\partial t}=[\phi-\Delta\lambda\,\theta(1-\phi^2)](1-\phi^2)+\nabla\cdot(w^2\nabla\phi)-\frac{\partial}{\partial x}\left(w\frac{\partial w}{\partial\zeta}\frac{\partial\phi}{\partial y}\right)+\frac{\partial}{\partial y}\left(w\frac{\partial w}{\partial\zeta}\frac{\partial\phi}{\partial x}\right), \tag{6}$$

where τ and λ are constants chosen according to Karma and Rappel [20,21], to impose the modified Gibbs-Thomson condition. The solid-liquid interface has a dimensionless thickness of order unity, but the values of τ and λ depend on the length scale W.

The pure metal used in the simulations is assumed to have a body-centered cubic lattice, with a fourfold anisotropy of the surface energy at the solidification interface. This enters the phase-field equation (6) via the function w, which is chosen here as

$$w=1+\epsilon\cos[4(\zeta-\zeta_0)], \tag{7}$$

where ζ is the angle between the normal of the solid-liquid interface and the vertical direction, and ϵ is the degree of anisotropy in the surface energy.

In the simulations it is assumed that the lattice of the nucleus has an arbitrary orientation, and that this orientation is controlled by the parameter ζ_0. This results in the situation that, without any flow, one of the main branches would eventually grow in the direction given by ζ_0, as shown in Fig. 1, where $\zeta_0=45°$. The angle ζ is calculated using the spatial derivatives of ϕ, according to:

$$\zeta=\arctan\left(\frac{\partial\phi}{\partial y}\Big/\frac{\partial\phi}{\partial x}\right). \tag{8}$$

III. NUMERICAL METHOD

The numerical method employed in the present paper is the same as that in Refs. [27,28], where more details were reported. The addition of the buoyancy term in the momentum equations do not add any fundamentally new numerical difficulties. We will thus discuss numerical issues only briefly.

The main features of our numerical strategy is that we use a Galerkin formulation of the finite element method, with piecewise linear base functions and unstructured meshes of triangular elements. The spatial resolution of the mesh changes adaptively during the computation to obtain an accurate solution with a minimal number of elements. The adaptivity in the present paper is accomplished by making a coarse initial mesh and then adaptively splitting or merging the elements according to an error indicator.

A rather large domain was used to reduce the influence of the walls. The same dimensionless domain size was used for all cases. It extends between 0 to 60000 in the x direction, and -60000 to 60000 in the y direction, and the finest and coarsest resolutions are about 0.45 and 5000, respectively.

The reference length W was chosen in order to reflect the tip length scales, in such a way that the nondimensional tip radius should be around 12. Consequently it is taken differently depending on the undercooling. In Sec. IV we will discuss five different values of the nondimensional undercooling, $\Delta = 0.08$, 0.04, 0.02, 0.01, and 0.005. The corresponding values for the reference length are $W = 140.8 d_0$, $500 d_0$, $1000 d_0$, $1666.66 d_0$, and $3333.33 d_0$, where d_0 is the capillary length $d_0 = c_p \sigma_0 T_m / L^2$.

A typical element distribution consists of about 150000 elements and 75000 nodes. Most of the elements resolve the interface region; therefore, the number of elements and nodes scale with the arclength of the solid-liquid interface, at all times. This mesh corresponds to the computation with $\Delta = 0.02$, also shown in Fig. 4(b) and it took about 300 CPU hours on a CRAY J932 (1 CPU). The corresponding case without convection needs about half of this CPU time.

To solve the Navier-Stokes system of equations, a scheme proposed by Gresho *et al.* [30] was used. In accordance with this we employ pressure splitting and a streamline-upwind Petrov-Galerkin treatment of convective terms. The discretized systems of equations were solved using conjugate gradients or GMRES, as appropriate. Diffusive terms were treated implicitly. For the low undercooling cases ($\Delta \leqslant 0.02$), the convective terms were also implicit.

The Navier-Stokes solver has been validated, among other test cases, for flow past a circular cylinder, where the computed wake length and position of wake center were compared with those by Fornberg [31] for $\mathrm{Re} = 10 - 200$. In these tests the cylinder was represented by the use of a prescribed phase field, in order to test the implementation of the no slip condition on the crystal. The seemingly crude method of increasing viscosity, as given in Eq. (5), was found to be quite adequate. This is understandable, since the flow fields are quite viscous here, and thus vary over the length scale of the size of the crystal, while the thin region around the interface is extremely well resolved. More details were given in Refs. [27,28].

The time step dt is controlled by the inequalities $dt V_\phi \leqslant 0.001$ and $dt \leqslant 5$, where V_ϕ is the maximum normal speed of the interface. These criteria result such that when the time step is decreased by a factor of 10 for a case with $\Delta = 0.08$, the relative difference in position and velocity of the interface caused by the change in time step is never larger than 1% (for time $\leqslant 4 \times 10^5$). For a typical run, the time step is initially 10^{-4}; it then increases slowly, with less than $\leqslant 0.05\%$ per time step.

To validate our code and adjust the error indicator we compared our simulations with published simulations. First the convection was turned off, and we made a comparison with the results by Karma and Rappel [20] and Provatas [32]. For $\Delta = 0.25, 0.45$, and 0.55 our results agree, within a few percent relative error. We have concluded that the radius of the tip, R, should be at least around seven length scales W, and the resolution should be 0.44 or finer to obtain an accuracy within a few percent. In the simulations presented below, the length scales were selected to give $R \geqslant 12W$.

At undercooling below 0.25 we did not have access to reference solutions to compare with, but our experience from using different interface widths, meshes, etc. is consistent with the rule that the radius of curvature should not be less than approximately 12 interface widths. The requirement that the radius of curvature should be larger than the interface width also seems to be the most restrictive of the four conditions given by Karma and Rappel [20] for the validity of their second order accurate version of the phase-field equations.

In the related Hele-Shaw cell problem, Folch *et al.* [33,34] found that the accuracy of the growth of linear instabilities was affected by the capillary length scale, since the spontaneous wavelength scales with the capillary length. The critical wavelength, however, also increases with decreasing undercooling, so that, despite the seemingly very large ratios W/d_0 that are used here, the critical wavelengths are actually resolved. Indeed, the essence of the marginal stability theory is that the tip radius should be comparable to the critical wavelength; i.e., if the tip radius is resolved, then the critical wavelength is also resolved.

The implementation of the mathematical problem was done by using and developing code generation tools that automatically create a FEM code from a symbolic high level representation of the partial differential equations [35]. This makes it possible to handle the complicated mathematical models that are used here in an intuitive manner, and greatly reduces the work required for implementing different models and formulations.

IV. RESULTS

Five different values of the dimensionless undercooling — Δ, 0.08, 0.04, 0.02, 0.01, and 0.005 — have been investigated. This corresponds to values of the undercooling between 1.92 and 0.12 K, which is in the range of experiments.

Figure 2 shows the flow field around the crystal for $\Delta = 0.02$, at a nondimensional time 1.64×10^6. The reference length scale here is $W = 1000 d_0$. Note that only a small fraction of the nodal velocities are shown. Figure 2(b) shows the flow field in the vicinity of the crystal. The flow is clearly an upward natural convection, driven by the release of latent heat as the crystal grows. Figure 2(a) shows the flow field in

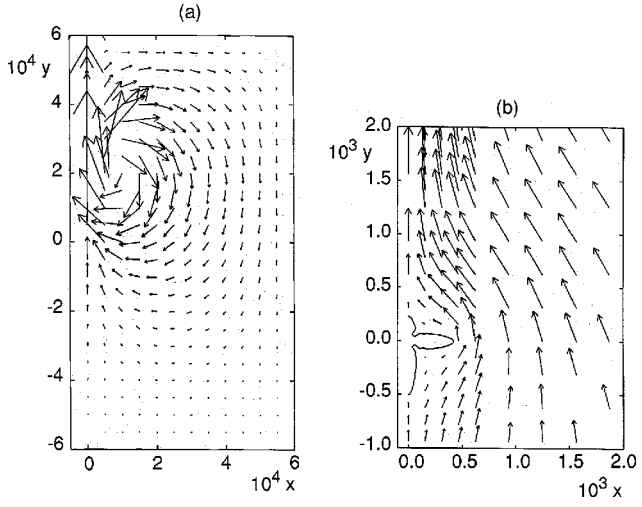

FIG. 2. Flow field around a growing crystal. (a) Entire domain. (b) Close up around the crystal.

the entire domain. The flow is directed toward the crystal from below and from the sides. The fluid that is heated near the crystal forms a plume, which rises vertically above the crystal.

The nominal Rayleigh number Ra, based on the reference length W, has the value 2.24×10^{-7}. A more representative Rayleigh number is obtained by basing it on the dendrite arm length l (nondimensional) instead. For this case this gives, using the length of the downward growing arm $l=500$, $\mathrm{Ra}_l = l^3\mathrm{Ra}=27.8$. This is consistent with the convective flow pattern that we see. With this low Ra, and also for the rather large Pr used here, the flow is quite viscous, and there is no distinct fluid flow boundary layer. The upward flow extends to distances from the crystal that are significantly larger than the dendrite arm length.

The rising plume above the crystal eventually reaches the top of the container, and will start to build up a stratification. However, this has not yet happened at the time shown in Fig. 2. The plume is still evolving, and the heated fluid has only reached a certain height, roughly coinciding with the center of the vortex seen in Fig. 2(b) (around height 20000).

The fluid in the plume continues to accelerate above the crystal, giving a flow velocity which is maximal on the centerline far above the crystal. In Fig. 2(a) the maximum fluid velocity is 0.055, while the growth velocity of the downward growing branch is 0.00029. This implies a fluid velocity that is almost 190 times faster than the growth velocity, but it should be remembered that the fluid velocity is much lower at the tip of the downward growing branch.

Figure 3 shows the thermal field corresponding to the flow fields in Fig. 2. The temperature has returned to the undisturbed initial value at a distance from the crystal which is approximately the overall crystal size. This is consistent with the small value of Ra_l, but the isotherms also reveal clear convective effects. Above the crystal the beginning of the thermal plume is visible. Comparing with the flow field in Fig. 2, it is evident that the velocity disturbance reaches much further from the crystal than the temperature disturbance. This is to be expected in any high Prandtl number natural convection flow.

The isotherms reveal that the heat flux is increased at the tip of the downward growing branch, while it is decreased at the upward growing branch. The growth Peclet number is defined as $P=VR/2$, where V and R are the nondimensional tip growth velocity and radius, respectively. The value of the growth Peclet number is around 0.00172 for the tip of the

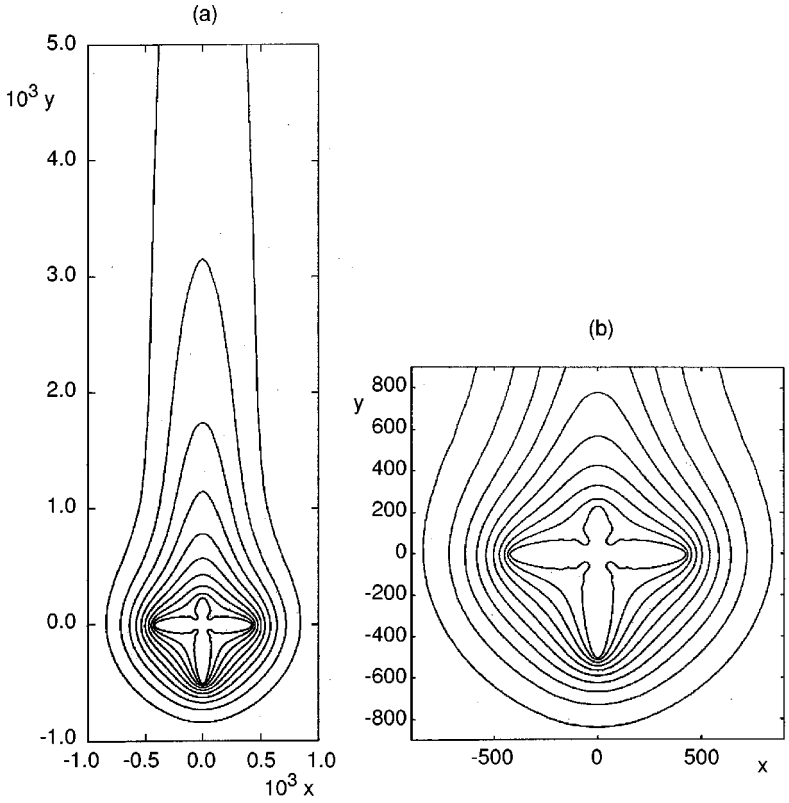

FIG. 3. Isotherms around a growing crystal. (a) The vicinity of the crystal. (b) Close up around the crystal.

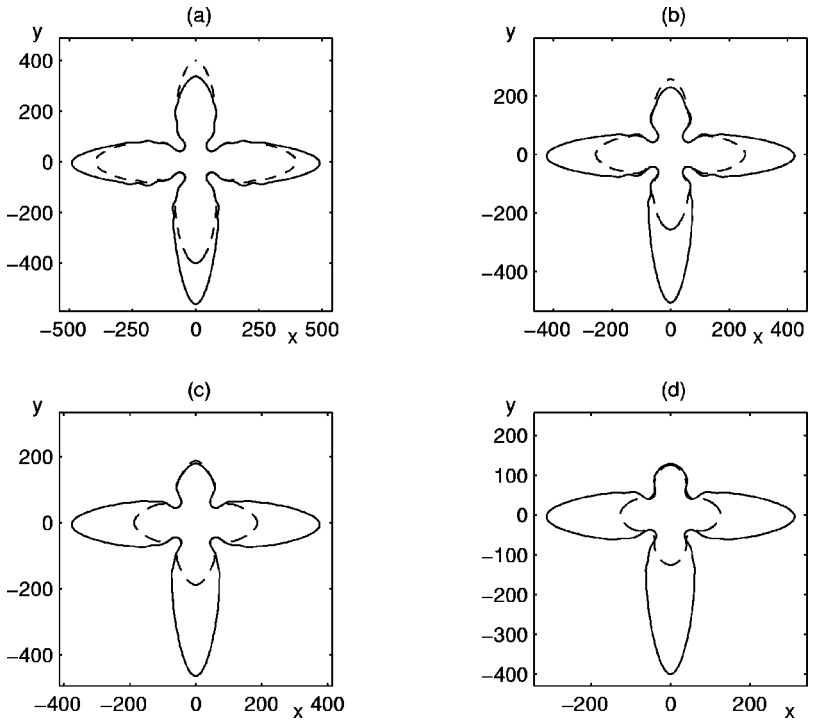

FIG. 4. Solid-liquid interfaces at different values of undercooling: (a) $\Delta = 0.04$, (b) $\Delta = 0.02$, (c) $\Delta = 0.01$, and (d) $\Delta = 0.005$.

downward growing branch. The convective effects that can be seen in the shape of the isotherms are thus not the consequence of the translation of the tip, but instead of the fluid motion. This observation is also supported by the fact that the flow velocity below the crystal is larger than the tip growth velocity (a factor 6 higher at a distance 100 below the downward growing tip).

In Fig. 4 the results for four different undercoolings are shown. The dashed and solid lines represent the solid-liquid interface without and with natural convection. The reference length W was chosen to reflect the tip radius of the downward growing branch, so that the nondimensional tip radius was around 12. In the four cases $\Delta = 0.04$, 0.02, 0.01, and 0.005, W was taken as $500d_0$, $1000d_0$, $1666.66d_0$, and $3333.33d_0$, respectively. Each case was simulated in time to produce a main downward branch that was approximately of the same nondimensional length; 400–500. This choice, together with the choice of reference length in terms of actual tip radius, means that even though the actual size and time for growth is very different between the different cases, all cases show dendrites that are of a similar geometric complexity, in terms of the ratio between size and tip radii.

A general trend is that the velocity of the tip of the downward growing branch increases due to the flow. The increase becomes larger as the undercooling is reduced, due to the fact that the size of the crystal becomes larger, and thereby the natural convection is enhanced. The main flow in the vicinity of the crystal is directed upwards which results in that the flow enhances the heat transfer most at the downward growing branch of the crystal, and it is always this branch that grows the fastest.

The shapes in Fig. 4(a), for $\Delta = 0.04$, were obtained at a time 1.28×10^6. The nondimensional velocity and tip radius of the downward branch in the convecting case are $V = 3.9 \times 10^{-4}$ and $R = 14.75$, respectively. It is seen that the downward and the horizontal branches have grown 20–30 % longer in the convecting case than in the nonconvective. There is thus a clear influence on growth from convection. For this case the Rayleigh number based on a dendrite arm length $l = 563$, is $\mathrm{Ra}_l = l^3 \mathrm{Ra} = 9.90$.

Figure 4(b) shows the comparison between the crystal shapes with and without convection for $\Delta = 0.02$, at the same time, 1.64×10^6, as was shown in Figs. 2 and 3. The tip velocity and radius of the downward growing convective branch is 2.87×10^{-4} and 12, respectively. The overall size Rayleigh number was here $\mathrm{Ra}_l = 27.8$. The comparison between the convecting and nonconvecting cases now shows that convection has more than doubled the length of the downward and horizontal branches, leaving the upward branch slightly shorter.

At $\Delta = 0.01$ [Fig. 4(c)], taken at time 2.55×10^6, this trend is even more pronounced. The dendrite arm length Rayleigh number here is $\mathrm{Ra}_l = 52.3$, based on the actual length of the lower arm $l = 467$. This increased value of the Rayleugh number clearly reflects the increased convective effects on the growth which are evident in Fig. 4(c). The downward and horizontal branches are even more enhanced, with the downward branch the longest. The tip speed and radius of the downward branch are 1.7×10^{-4} and 12.3, respectively. The upward growing branch almost coincides with the nonconvecting one.

The largest difference between the convective and nonconvective cases occurs for the lowest undercooling $\Delta = 0.005$, shown at time 3.10×10^6 in Fig. 4(d). The tip velocity and radius are 1.2×10^{-4} and 10, respectively. The overall size Rayleigh number is now $\mathrm{Ra}_l = 132$, based on the lower arm length $l = 400$. This again confirms the increasing effect of natural convection as the undercooling is decreased.

As an example of the other extreme, where convection becomes unimportant, the case with $\Delta = 0.08$ (not shown) was computed. The convection gives slightly different tip velocities for the branches, but the difference in relative tip velocity is only 3.5% at time of 6×10^5. The downward

growing branch has reached about $y=420$, and the velocity and radius of the tip are 4.5×10^{-4} and 26, respectively. The overall size Rayleigh number is $\mathrm{Ra}_l=0.185$. Compared to the case without convection, the relative difference in vertical position of the lower tip is less than 1%, and the convective and nonconvective shapes are indistiguishable. Hence at this undercooling the effect of the thermal natural convection on the crystal growth is negligible.

The time history for the growth velocity for the downward growing branch is interesting. In all cases without convection the growth does not reach a steady state. This is expected at these low undercoolings, since in the presence of very slow growth, the convective effects due to the motion of the solidification front are largely absent. The thermal field will then evolve in time as pure diffusion from a localized heat source. In two dimensions, as is well known, the far field is logarithmic, and a steady state is possible only after the diffusion has reached the outer boundary. Provotas *et al.* [26] investigated the scaling of this time dependent growth at undercoolings as low as $\Delta=0.05$. Both with and without convection, there is an initial transient when the initial condition for temperature is equilibrated over a length scale comparable to the size of the initial nucleus.

However, with convection the growth velocity soon reaches a quasi-steady-state. With the natural convection flow the diffusion of heat is balanced by the convective removal of heat, and the disturbance of the temperature field is confined within a region which for the higher Rayleigh numbers starts to resemble a convective boundary layer of thickness $l\mathrm{Ra}_l^{-1/4}$.

With convection the time history of the tip downward growth is typically that, after an initial rapid growth, the tip speed drops to an almost constant value. This may typically increase slightly at later times. This is due to the fact that the size of the crystal is continually increasing, and this causes a continued increase of the natural convection, but this is a minor effect as the growth velocity of the tip is increasing very slowly.

For $\Delta=0.04$, the velocity is increasing at the time shown in Fig. 4(b). However, the increase in speed is very slight, during the last 100 length units of growth, the speed of the downward growing tip increased only by 1.2%. Similarly, for $\Delta=0.02$ and $\Delta=0.01$, at the times shown in Figs. 4(c) and 4(d), respectively, the tip speeds have been decreasing but have just started to increse slightly. For $\Delta=0.005$, at time 3.10×10^6 in Fig. 4(d), the tip velocity has increased by 2% during the time required for growth over the last 100 length units. The steady state tip velocity is not strictly reached, but the change is very slow and can practically be interpreted as steady state. For $\Delta=0.08$, as discussed above, convection effects are negligible. Consequently no steady state tip velocities were obtained for this undercooling.

The slow increase of growth velocity with crystal size is understandable as a consequence of an increasing flow speed around the tip, as the crystal grows in size. With a larger crystal the velocity scale of the convective motion increases. The tip will thus experience an increased convective flow which will give an enhanced heat transfer. Note that, if the tip had been so large that there had been well resolved boundary layers around it, the flow would be self-similar, and the local heat transfer at the tip would be independent of the overall crystal size. Here, however, the tip region is very small, and indeed there is no self similar boundary layer region at all. A reasonable conceptual model for the heat transfer at the tip would rather be a small object in a forced flow, where the flow is driven by the convection on the dendrite size scale.

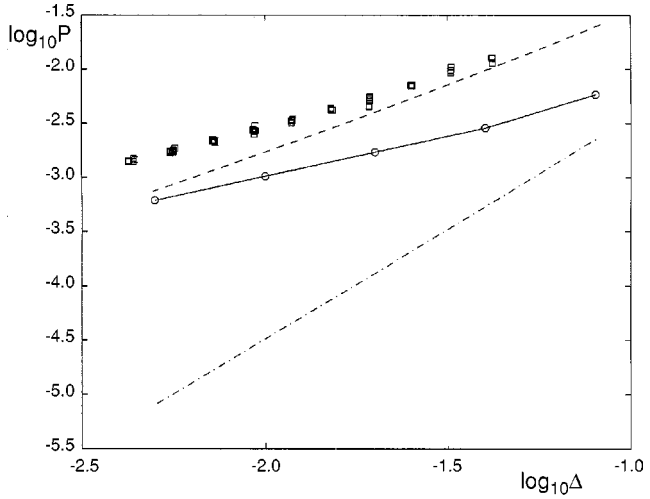

FIG. 5. Growth Peclet number vs nondimensional undercooling. The solid line shows the present simulations; the dashed line shows a 3D Ivantsov construction; squares are experimental results by Glicksman [4]; and the dash-dotted line shows a 2D Ivantsov construction.

The flow also increases the growth of the horizontal branch. This branch has grown 87%, 83%, 81%, and 77% of the length of the downward growing branch for $\Delta=0.04,0.02,0.01$, and 0.005, respectively. This difference in length is observed to slowly increase as time elapses, because the difference in velocities of these branches is still slowly increasing.

The flow is viscous for all values of the undercooling and the main flow follows the solid-liquid interface, without separated flow regions. The vortex that was observed in the case $\Delta=0.02$ (Fig. 2) has, for $\Delta=0.01$ and 0.05, reached the upper wall, and is developing into the overall circulation in the chamber. Still the temperature is undisturbed away from the plume and the crystal. Hence there are not yet any strong effects of the finite size of the chamber, and we do not expect the results to be sensitive to a change in chamber size.

With convection the stability (selection) parameter $\sigma=1/(PR/(d_0/W))$ is 0.047–0.048, where d_0 is the capillary length and $P=VR/2$ is the growth Peclet number, where V and R are the nondimensional tip growth velocity and radius, respectively. This value is more than twice the value of 3D experiments with SCN, and some of this difference is probably due to that here the value of the anisotropy parameter ϵ that was used is a bit high.

Figure 5 shows the growth Peclet numbers P for the simulations as a function of the undercooling. In the graph, the dash-dotted and dashed lines are the growth Peclet numbers according to an Ivantsov solution without convection in two and three dimensions, respectively. The squares are experimental results for SCN in a terrestrial enviroment found by Glicksman [4]. The most striking feature is that the growth Peclet number increases with the undercooling in very much

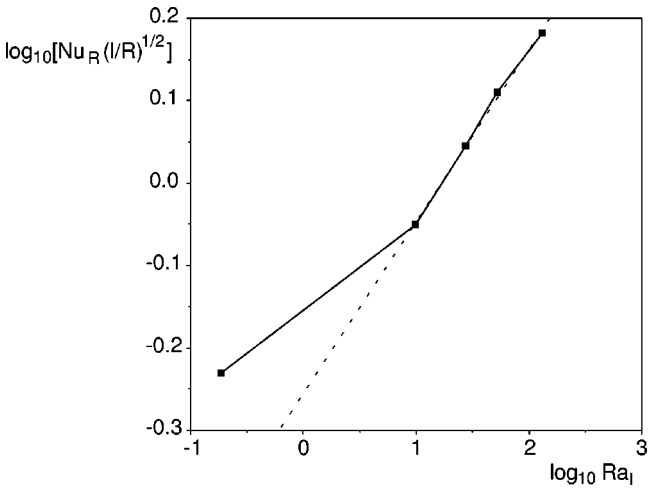

FIG. 6. Relation between tip Nusselt number and overall Rayleigh number. The solid line and squares show the present simulations; the dashed line is a fit to the data with $\Delta \leqslant 0.04$, giving the relation $\mathrm{Nu}_R(l/R)^{1/2}=0.555\,\mathrm{Ra}_l^{1/4.79}$.

the same way for our simulations and the experiments, despite the fact that the simulations are 2D.

The large difference between the 2D and 3D Ivantsov curves in Fig. 5 are due to the logarithmic far field singularity in a 2D diffusion problem, which is absent in three dimensions. However, with convection a finite length scale for the thermal field is established, and the heat transfer becomes independent of the state far from the crystal; this also holds in the 2D case. There is a quantitative difference between simulation results and experimental results, but that is a constant factor, the slope of the curves agree quite well. This indicates that the essential features of the convective effects are similar in the experiments and the 2D simulation.

Some of the difference could also be due to the fact that the assumed anisotropy value $\epsilon=0.015$ is a bit high for SCN. Wheeler *et al.* [36] showed that the growth Peclet number for diffusion controlled growth increases with decreasing values of ϵ.

Figure 6 shows the relation between a Nusselt number for the downward growing branch and the Rayleigh number. The Nusselt number is based on the tip radius and the release of latent heat, which should be the relevant scales governing the heat transfer around the tip. This gives an expression of $\mathrm{Nu}_R=VR/\Delta$, where V and R are the nondimensional tip growth speed and radius, as above. Using the argument outlined above in connection with the discussion of the time dependence of the growth, we expect the heat transfer around the tip to be governed by the flow caused by the overall natural convection. This would give $\mathrm{Nu}_R \approx \mathrm{Pe}_R^{1/2}$, where $\mathrm{Pe}_R = UR$ is a Peclet number based on the flow velocity U (nondimensional) and the tip radius. This flow velocity is assumed to be driven by the overall convection, i.e., $U \approx \mathrm{Ra}_l^{1/2}/l$. This gives a relation between Nu_R and Ra_l according to $\mathrm{Nu}_R(l/R)^{1/2} \approx \mathrm{Ra}_l^{1/4}$.

This relation has been tested in Fig. 6. It is seen that $\log_{10}[\mathrm{Nu}_R(l/R)^{1/2}]$ varies linearly with $\log_{10}(\mathrm{Ra}_l)$, as expected, except for the lowest value of Ra_l corresponding to $\Delta=0.08$, where we do not expect convection to be important. With this choice of parameters it is also clear that the switchover from convectively to diffusively controlled growth occurs for $\mathrm{Ra}_l \approx 1$. A fit of a power law to the points where convection dominates gives the result that $\mathrm{Nu}_R(l/R)^{1/2}=0.555\,\mathrm{Ra}_l^{1/4.79}$, in reasonable agreement with the expected law. It is an attractive feature of this relation that it involves both the tip radius and the overall length scale; however, in view of the limited parameter range that was covered, we do not wish to overemphasize the significance of this.

The preferred growth direction was also changed 45° for $\Delta=0.02$ and $\Delta=0.005$, i.e., ζ_0 was set to 45° in these two simulations. These cases were compared to the corresponding cases with the same undercoolings and $\zeta_0=0$. Without flow the results were of course independent of this variation in ζ_0, as expected; thus the initial transient was the same. With flow the two ζ_0 values give different flow picture in the vicinity of the crystal. When $\zeta_0=45°$ degrees there are two downward branches that are growing with 45° angles relative to the gravity vector. Between these branches the melt is warm, but it is prevented from flowing upward by the crystal, and as a result this is almost a stagnant region. Still, the change in the flow field has only small effects on the growth velocity of the downward branches. The tip velocity for these downward branches is only marginally smaller than the tip velocity for the downward growing branch with $\zeta_0=0°$. For both undercoolings the increase of ζ_0 resulted in less than 1% relative change in tip velocity.

In the cases $\Delta=0.005$ and $\zeta_0=45°$, the upward growing branches grow with 60% of the velocity of the downward growing branches and their growth direction are 5° upstream relative to the respective preferred growth direction. Moreover, the tip shape of an upward growing branch is no longer parabolic. The downstream side of the tip is less curved, even though the main flow follows the solid-liquid interface around the tip. Hence the flow has asymmetrically increased the heat flux at this tip.

All cases above are for the terrestrial value of the gravitation, but two simulations were also done with reduced gravitation. For $\Delta=0.005$, gravitation was reduced by factors of 10^3 and 10^6. The results were that the crystal is still affected by the natural convection in case of the 10^3 reduction, but unaffected for the 10^6 reduction. Still, for the 10^6 reduction, the size of the envelope enclosing the crystal was less than 200, and there might be some small convective effects that appear at larger times.

V. CONCLUSION

Realistic parameter values for SCN and undercoolings down to 0.12 K were used to simulate effects of natural convection on crystal growth. The natural convection becomes stronger and affects the crystal growth more as the undercooling decreases, due to the increase in size of the crystal with decreasing undercooling. For undercoolings larger than 1.92 K the natural convection has only a small effect on the crystal growth, as expected from previous experiments. When the growth Peclet number for the simulations with natural convection are compared with results from terrestrial experiments, a similar dependency on undercooling is observed, despite the fact that the simulations are 2D, and the experiments are 3D.

With one preferred growth direction aligned with gravity,

the downward growing branch is always the fastest growing one. The growth of the horizontal branches are also increased by the natural convection. The velocity of these branches are more than 75% of the velocity of the downward growing branch, and the difference in growth velocity increases with lower undercooling. This growth is faster than diffusion dominated growth. On the other hand, the upward growing branch grows with a lower velocity than in the case of diffusion dominated growth.

When the preferred growth direction was set at a 45° angle from the vertical direction, the growth velocity of the branches that grow downward was not affected; hence the growth velocity was the same as for a downward growing branch, with the preferred direction aligned with gravity. The branches that grow at 135° relative to gravity grow with 60% of the velocity of the downward growing branches. This dependency of the growth on the orientation relative to gravity is also observed in experiments, where the growth velocity for moderate undercooling is rapidly decreased as the growth direction exceeds a 110° angle with respect to the gravity vector.

In simulations with convection, the growth velocity of the downward growing tip becomes almost constant, over a modest range of crystal sizes. The growth was correlated to a Rayleigh number based on overall crystal size. In this correlation, the growth would depend both on the tip radius and the size of the envelope of the crystal.

The stability parameter σ becomes about twice as large as in the experiments for cases with flow. With convection, the stability parameter has a variation of 2% and this small variation does not correlate with the undercooling. Therefore, with convection, the stability parameter is independent of the undercooling and the fluid flow for the range of undercooling used here.

ACKNOWLEDGMENT

This work was supported by the Swedish Research Council for Engineering Science (TFR).

[1] Y.-W. Lee, R. N. Smith, M. E. Glicksman, and M. B. Koss, in *Annual Review of Heat Transfer*, edited by C.-L. Tien (Begell House, New York, 1996), Vol. 7, pp. 59–139.
[2] M. E. Glicksman, M. B. Koss, and E. A. Winsa, Phys. Rev. Lett. **73**, 573 (1994).
[3] M. E. Glicksman, S. R. Coriell, and G. B. McFadden, Annu. Rev. Fluid Mech. **18**, 307 (1986).
[4] M. E. Glicksman, M. B. Koss, L. T. Bushnell, J. C. LaCombe, and E. A. Winsa, ISIJ Int. **35**, 1216 (1995).
[5] J.P. Kallungal and A.J. Barduhn, AIChE J. **23**, 294 (1977).
[6] J.S. Huang and A.J. Barduhn, AIChE J. **31**, 747 (1985).
[7] Y.-W. Lee, Ph.D. thesis, Rensselaer Polytechnic Institute, 1991.
[8] M. B. Koss, L. T. Bushnell, J. C. LaCombe, and M. E. Glicksman, Chem. Eng. Commun. **152-153**, 351 (1996).
[9] R. Ananth and W. N. Gill, J. Cryst. Growth **91**, 587 (1988).
[10] G. P. Ivantsov, Dokl. Akad. Nauk. SSSR **58**, 567 (1947).
[11] V. Pines, A. Chait, and M. Zlatkowski, J. Cryst. Growth **167**, 383 (1996).
[12] G. B. McFadden and S. R. Coriell, J. Cryst. Growth **74**, 507 (1986).
[13] R. Ananth and W. N. Gill, J. Cryst. Growth **179**, 263 (1997).
[14] R. F. Sekerka, S. R. Coriell, and G. B. McFadden, J. Cryst. Growth **171**, 303 (1997).
[15] L. A. Tennenhouse, M. B. Koss, J. C. LaCombe, and M. E. Glicksman, J. Cryst. Growth **174**, 82 (1997).
[16] Y.-W. Lee, R. Ananth, and W. N. Gill, Chem. Eng. Commun. **116**, 193 (1992).
[17] Y.-W. Lee, R. Ananth, and W. N. Gill, J. Cryst. Growth **132**, 226 (1993).
[18] D. Canright and S. H. Davis, J. Cryst. Growth **114**, 153 (991).
[19] R. F. Sekerka, S. R. Coriell, and G. B. McFadden, J. Cryst. Growth **154**, 370 (1995).
[20] A. Karma and W. J. Rappel, Phys. Rev. E **53**, R3017 (1996).
[21] A. Karma and W. J. Rappel, Phys. Rev. Lett. **77**, 4050 (1996).
[22] X. Tong, C. Beckermann, and A. Karma, in *Modeling of Casting, Welding and Advanced Solidification Processes VIII*, edited by B. G. Thomas and C. Beckermann (The Minerals, Metals & Materials Society, Warrendale, PA, 1998).
[23] Nikolas Provatas, Nigel Goldenfeld, and Jonathan Dantzig, J. Comput. Phys. **148**, 265 (1999).
[24] A. Karma and W. J. Rappel, J. Cryst. Growth **174**, 54 (1997).
[25] R. J. Braun and B. T. Murray, J. Cryst. Growth **174**, 41 (1997).
[26] N. Provatas, N. Goldenfeld, J. Dantzig, J. C. LaCombe, A. Lupulescu, M. B. Koss, M. E. Glicksman, and R. Almgren, Phys. Rev. Lett. **82**, 4496 (1999).
[27] R. Tönhardt and G. Amberg, J. Cryst. Growth **194**, 406 (1998).
[28] R. Tönhardt and G. Amberg, J. Cryst. Growth **213**, 161 (2000).
[29] H. J. Diepers, C. Beckermann, and I. Steinbach, in *Solidification Processing 1997: Proceedings of the Fourth Decennial International Conference on Solidification Processing*, edited by J. Beech and H. Jones (University of Sheffield Press, Sheffield, 1997), pp. 426–430.
[30] P. M. Gresho, S. T. Chan, M. A. Christon, and A. C. Hindmarsh, Int. J. Numer. Methods Fluids **21**, 837 (1995).
[31] B. Fornberg, J. Fluid Mech. **98**, 819 (1980).
[32] N. Provatas (private communication).
[33] R. Folch, J. Casademunt, A. Hernandez-Machado, and L. Ramirez-Piscina, Phys. Rev. E **60**, 1724 (1999).
[34] R. Folch, J. Casademunt, A. Hernandez-Machado, and L. Ramirez-Piscina, Phys. Rev. E **60**, 1734 (1999).
[35] G. Amberg, R. Tönhardt, and C. Winkler, Math. Comput. Simul. **49**, 149 (1999).
[36] A. A. Wheeler, B. T. Murray, and R. J. Schaefer, Physica D **66**, 243 (1993).